Asymmetric Excitation of Surface Plasmon Polaritons via Paired Slot Antennas for Angstrom Displacement Sensing

Tianyang Zang,[1] Haofeng Zang,[1] Zheng Xi,[2] Jing Du,[1] Han Wang,[1] Yonghua Lu,[1,3,*] and Pei Wang[1,3,†]
[1]Department of Optics and Optical Engineering, University of Science and Technology of China, Hefei 230026, China
[2]Optics Research Group, Delft University of Technology, Department of Imaging Physics, Lorentzweg 1, 2628CJ Delft, The Netherlands
[3]Advanced Laser Technology Laboratory of Anhui Province, Hefei, Anhui 230026, People's Republic of China

(Received 21 February 2020; accepted 1 June 2020; published 16 June 2020)

Optical antennas enable efficient coupling between propagating light and bonding electromagnetic waves like surface plasmon polaritons (SPPs). Under the illumination of inhomogeneous optical fields, propagating SPPs mediated by multimode antennas could be spatially asymmetric and the asymmetry strongly depends on the position of the antennas relative to the illumination field. Here we develop such asymmetric excitation of SPPs through illuminating a pair of slot antennas with the (1,0) mode Hermite-Gaussian beam. The physical scenario of the interaction between the illumination optical field and the paired slot antennas are elaborated by full-wave electromagnetic simulations. We also carry out experiments to monitor the asymmetric SPPs propagation with a back-focal plane imaging technique. By retrieving the asymmetric intensity ratio of the SPP pattern in the back-focal plane image, lateral displacement of the antennas down to angstrom level is demonstrated.

DOI: 10.1103/PhysRevLett.124.243901

Introduction.—Optical metrology is of particular significance for it allows one to measure distance or displacement in a noncontact high-precision way [1]. The interferometric method has been well developed and widely applied to detect relative phase differences introduced by tiny longitudinal displacement [2]. Additionally, high-precision measurement of transverse displacement is also challenging and greatly demanded for the development of nanotechnology, such as single molecule tracking [3–7] and nanoscopy [8], as well as overlay metrology for the semiconductor fabrications [9,10]. Developing a high-resolution optical ruler [11,12] is a direct optical metrology for the measurement of transverse displace, however, suffering from the requirement of an ultrastable laser.

Recent works [13–17] of unidirectional scattering of resonant optical antennas have proven to be capable for nanoscopic position sensing with lateral resolution even down to angstrom regime. High-index dielectric antenna supports both electric and magnetic modes. Upon the interference of a longitudinal and a transverse dipole radiation, directional scattering perpendicular to the propagation of the incident light beam can be achieved as transverse Kerker's condition is met. Similar unidirectional scattering also occurs for paired metallic resonant antennas [18]. When the nanoantenna is placed inside an inhomogeneous field with phase or polarization singularities, its scattering characteristics depend strongly on the local-field distributions and are highly sensitive to the position of the nanoantenna within the illumination field [13,16–20]. Consequently, by looking at the dramatic changes of the far-field scattering pattern of the nanoantenna combined with the knowledge of the local field, a very sensitive method can be developed to localize the nanoantenna within the illumination field at a scale that is much smaller than the wavelength, which could be highly interesting for compact optical nanometrology.

However, all these schemes rely heavily on the detection of the scattering from one or paired resonant antenna, and the scattering power is very low because of the subwavelength size of the nanoantenna [13,14]. Moreover, the schemes generally require illumination using a high numerical aperture lens to increase the scattered power and, as a consequence, the incident beam with high divergence angle also enters the back-focal plane of the detection lens and partly overlaps upon the scattering field. Thus, it is challenging to retrieve the scattering signals in the back-focal plane of the objective even though a weak measurement technique is employed [20].

In this Letter, we present a novel technique based on directional excitation of surface plasmon polaritons (SPPs) other than directional scattering of the optical antennas to realize angstrom displacement measurement. Because of the near-field interference, directional SPPs can be excited by some well-designed nanostructures [21–26] and the directivity can be manipulated by controlling the polarization of incident light [27–30]. In our approach, a pair of optical slot antennas is employed to excite SPPs under the illumination of the focused Hermite-Gaussion (HG) (1,0) mode light. The near-field interaction between slot antennas and the rapid amplitude variation of the incident light

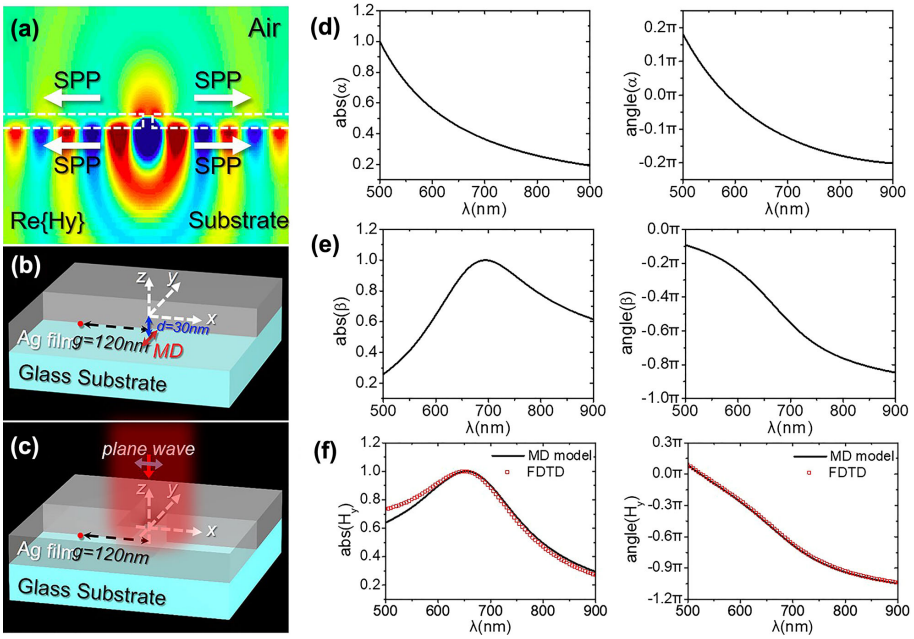

FIG. 1. Surface plasmon polaritons excited by single slot antenna. (a) Near-field magnetic field (H_y) distribution in cross section scattered from the rectangular slot antenna are simulated by finite difference time domain (FDTD). SPPs are excited at both upper and lower surface of silver film. (b),(c) Schematic illustrations of simulation models of surface plasmon polariton excited via (b) magnetic dipole source M_y and (c) rectangular slot under the illumination of x-polarized plane wave. (d) Amplitude (left) and phase (right) of coupling coefficient α is retrieved by simulating SPPs excited by an unit magnetic dipole and monitoring the near-field magnetic field 120 nm away. (e) The susceptibility β of the slot antenna is calculated by monitoring the far-field scatting from the slot under plane wave illumination. The amplitude (left) of β is resonant around 700 nm and the phase (right) of β is in the range of about $-\pi \sim 0$. (f) The near-field magnetic field is retrieved at the site 120 nm away from the slot based on the FDTD simulation (red circles). Both the amplitude (left) and phase (right) are compatible with the prediction of two-step model calculation of $\alpha \times \beta$ (black line).

create asymmetric SPPs when the paired slot antennas and the nodal line of the HG_{10} optical field is misaligned. The transverse displacement can be sensitively measured by detecting the SPPs leakage at the back-focal plane of an oil-immersed objective. Since the SPPs leakage pattern is spatially separated from the forward scattering of the slot antennas in the back-focal plane, the displacement signal can be monitored in almost dark background.

Results.—The rectangular slot in metallic film, termed as slot antenna, can be regarded as a complementary screen of a metallic nanorod that is generally considered as an electric dipole antenna. According to vector Babinet's principle [31], the scattering of slot antenna illuminated by perpendicular polarization is equivalent to the radiation of a magnetic dipole oriented in parallel, which is corroborated by comparing the far-field electromagnetic fields of a magnetic dipole with the simulations of a slot antenna (see Fig. S1 in the Supplemental Material [32]). It is reasonable to assume that induced magnetic dipole moment of the rectangular slot antenna by the incident light reads $\boldsymbol{m} = \beta \boldsymbol{H}_{\mathrm{loc}}$, where β represents the susceptibility of the slot antenna and $\boldsymbol{H}_{\mathrm{loc}}$ is the local magnetic field at the site of the slot antenna. Different from the nanorod antenna, slot antenna not only scatters the incident light to far field but also couples part of the light into the SPPs along the upper and lower surface of metal film [Fig. 1(a)]. The magnetic field of the SPPs is reasonably expressed as $\boldsymbol{H}_{\mathrm{SP}} = \alpha \boldsymbol{m}$ (see Sec. 1A in the Supplemental Material [32] for details). Here, we define α as coupling coefficient of a magnetic dipole exciting the SPPs along the metal film, which includes the contributions of coupling from the magnetic dipole radiation to SPPs and the propagation of SPPs along the metal surface.

To verify this interaction model, we simulate the SPPs excitation in two configurations: (A) a magnetic dipole source is embedded 5 nm underneath the metal film to excite the SPPs [Fig. 1(b)], and (B) a plane wave vertically illuminates the rectangular slot (120×50 nm) etched on a 50-nm-thick silver film to excite SPPs [Fig. 1(c)]. The surface electromagnetic field is monitored 120 nm away from the source point in x direction, which corresponds to the location of the other slot antenna in the following discussions. Figure 1(d) gives the coupling coefficient α of the slot antenna calculated from the scattering magnetic far field in configuration A (details of the calculation can be found in Sec. 1B in the Supplemental Material [32]). Figure 1(e) presents the amplitude and phase of susceptibility β retrieved from the simulation in configuration B (for details of the calculation, see Sec. 1C in the Supplemental Material [32]). The amplitude and phase

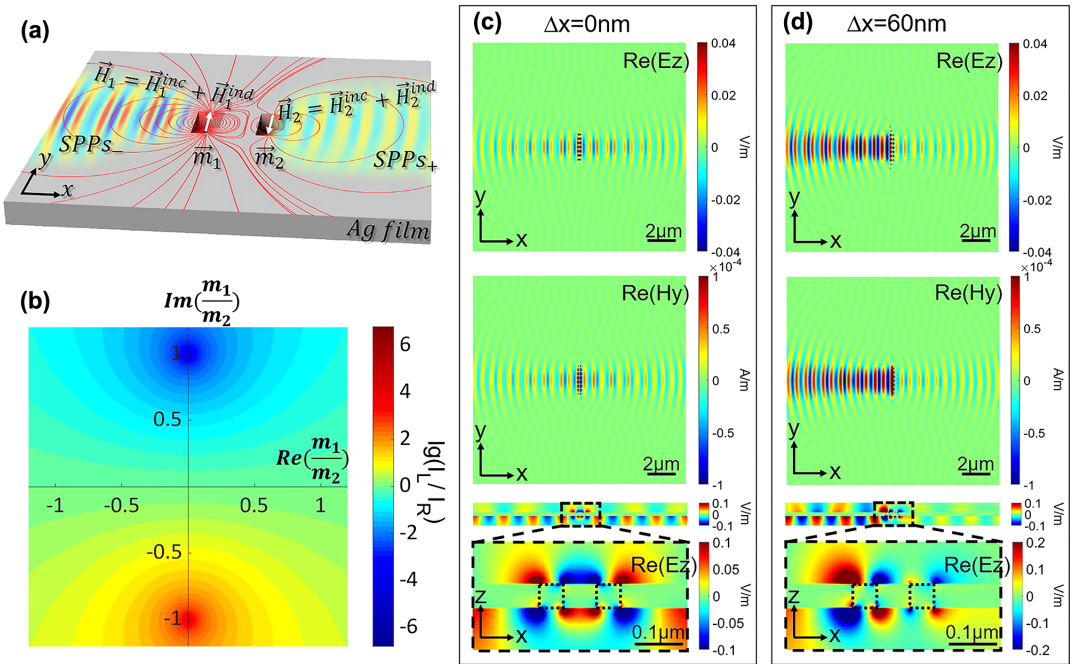

FIG. 2. Asymmetric SPPs excited arisen from the coupling between two adjacent slot antennas. (a) Schematic illustration of near-field coupling between the paired slot antennas and the asymmetric excitation of SPPs. Center-to-center distance of the two rectangular slots is $d = 120$ nm. (b) Logarithmic ratio of leftward SPPs over rightward SPPs is plotted in the complex plane of $\boldsymbol{m_1}/\boldsymbol{m_2}$. (c),(d) The near-field electromagnetic field distributions simulated under the illumination of HG_{10} mode beam, when the nodal line is (c) aligned to the center of POSAs and (d) shifted away $\Delta x = 60$ nm. The near-field electric field E_z (upper line) and magnetic field H_y (middle line) distributions are retrieved at the xy plane 10 nm above the metal surface. The lower line is the near-field electric field E_z in cross section and the dashed rectangles indicate the paired slots.

of the SPPs field $\boldsymbol{H}_y$ monitored at site 120 nm away from the source point [red circles in Fig. 1(f)] are well consistent with multiplication of $\alpha \times \beta$ [black line in Fig. 1(f)], which indicates that magnetic dipole approximation works well not only for the far-field scattering of slot antenna, but also the SPPs excitation mediated by slot antenna.

Figure 2(a) schematically shows a pair of rectangular slots etched on 50-nm-thick silver film deposited on silica substrate, termed as paired optical slot antennas (POSAs), to be employed to excite SPPs along the silver surface. The center-to-center distance of the POSAs is set as $d = 120$ nm in the simulation and experiment. Considering the electromagnetic coupling between the adjacent slot antennas, the effective magnetic dipole moment of the slot antenna m_1 and m_2 can be derived as (for details of the derivation, see Sec. 1A in the Supplemental Material [32])

$$\boldsymbol{m}_1 = \frac{\beta + \beta^2\alpha(\tilde{\boldsymbol{H}}_2^{\mathrm{inc}}/\tilde{\boldsymbol{H}}_1^{\mathrm{inc}})}{1-(\beta\alpha)^2}\boldsymbol{H}_1^{\mathrm{inc}}, \tag{1a}$$

$$\boldsymbol{m}_2 = \frac{\beta(\tilde{\boldsymbol{H}}_2^{\mathrm{inc}}/\tilde{\boldsymbol{H}}_1^{\mathrm{inc}}) + \beta^2\alpha}{1-(\beta\alpha)^2}\boldsymbol{H}_1^{\mathrm{inc}}, \tag{1b}$$

where $\tilde{\boldsymbol{H}}_{1,2}^{\mathrm{inc}}$ is the complex amplitude of the magnetic field ($\boldsymbol{H}_{1,2}^{\mathrm{inc}}$) of incident light at the site where the slots are located. Therefore, the surface plasmon optical wave excited by the POSAs is equivalent to the superposition of the optical fields that the magnetic dipoles $\boldsymbol{m_1}$ and $\boldsymbol{m_2}$ radiate. Consequently, the intensity of the left- or rightward SPPs waves from excited from POSAs can be written as

$$I_{\mathrm{left}} \propto |\boldsymbol{m}_1|^2 + |\boldsymbol{m}_2|^2 + 2|\boldsymbol{m}_1||\boldsymbol{m}_2|\cos(\Delta\Phi - kd), \tag{2a}$$

$$I_{\mathrm{right}} \propto |\boldsymbol{m}_1|^2 + |\boldsymbol{m}_2|^2 + 2|\boldsymbol{m}_1||\boldsymbol{m}_2|\cos(\Delta\Phi + kd). \tag{2b}$$

Here, $\Delta\Phi = \arg(\boldsymbol{m}_1) - \arg(\boldsymbol{m}_2)$ is the relative phase difference between the magnetic dipole momentums $\boldsymbol{m_1}$ and $\boldsymbol{m_2}$ that depends on both the converting coefficient $(\alpha \times \beta)$ of the slot antenna and the ratio $(\tilde{\boldsymbol{H}}_2^{\mathrm{inc}}/\tilde{\boldsymbol{H}}_1^{\mathrm{inc}})$ of the incident optical field located at the two slots. Supposing $kd = \pi/2$, Fig. 2(b) plots the logarithmic intensity ratio of leftward SPPs to rightward SPPs $\log(I_{\mathrm{left}}/I_{\mathrm{right}})$ depending on $\boldsymbol{m_1}/\boldsymbol{m_2}$ in the complex plane. It is seen that symmetric SPPs (i.e., $I_{\mathrm{left}} = I_{\mathrm{right}}$) is excited only when relative phase $\Delta\Phi = m\pi$, otherwise, SPPs arisen from the POSAs are asymmetric. Especially, when $\boldsymbol{m}_1/\boldsymbol{m}_2 = \pm\boldsymbol{i}$, that is, $\Delta\Phi = \pm\pi/2$, the ratio of left- to right-propagating SPPs intensity reaches maximum.

From Eqs. (1a) and (1b), the relative phase difference between the magnetic dipole momentums $\boldsymbol{m_1}$ and $\boldsymbol{m_2}$ reads

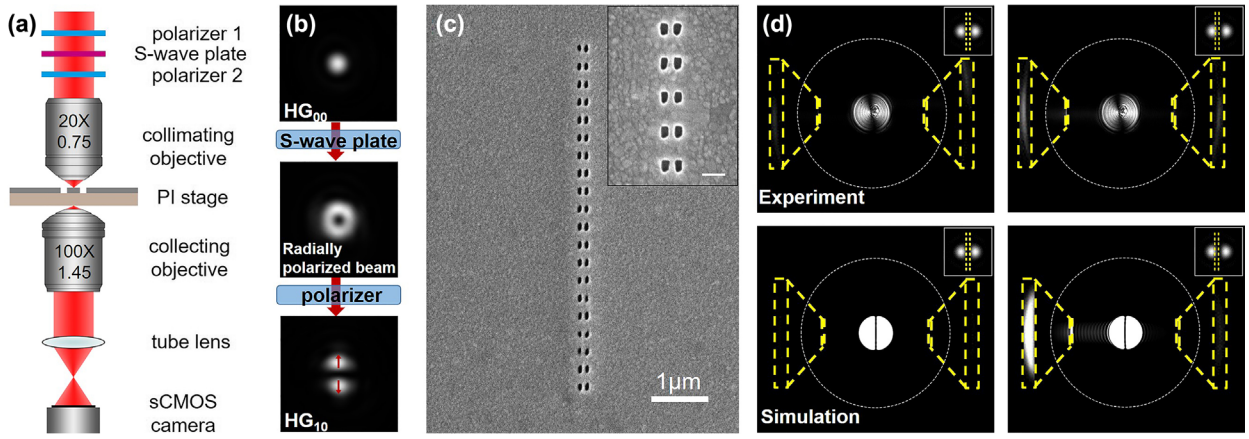

FIG. 3. Experiment setup and characteristics of optics and sample. (a) A collimated HG_{10} optical beam is focused by a microscope objective (20×, NA = 0.75) onto the POSA array. The antenna sample is mounted on a piezostage with nanometric resolution. The scattering field is collected by an oil-immersion objective (100×, NA = 1.45). The back-focal plane of the collecting objective is captured by a sCMOS camera. (b) The incident Gaussian beam (HG_{00} mode) is modulated by an *S*-wave plate to generate radially polarized beam and then passes through a polarizer to get a HG_{10} optical beam. (c) The SEM image of the antenna sample. The scale bar is 1 μm. (Inset) Amplified image of part of the paired slot array, and the scale bar is 200 nm. (d) Back-focal plane images acquired when the paired antenna is positioned in the center of HG_{10} optical mode (upper left) and shifted left 60 nm (upper right). The corresponding calculated back-focal plane images are compared in the lower left and right. The dashed white circles indicate the largest angles along which the radiated light can be collected by the oil-immersion objective. The dashed yellow rectangles represent the accumulated area to accumulate the intensity of SPPs.

$$\Delta\Phi = \arg\left(1 + \beta\alpha\frac{\tilde{\boldsymbol{H}}_2^{\mathrm{inc}}}{\tilde{\boldsymbol{H}}_1^{\mathrm{inc}}}\right) - \arg\left(\frac{\tilde{\boldsymbol{H}}_2^{\mathrm{inc}}}{\tilde{\boldsymbol{H}}_1^{\mathrm{inc}}} + \beta\alpha\right). \quad (3)$$

For a given POSAs structure, the relative phase $\Delta\Phi$ depends on the ratio of the incident optical field $(\tilde{\boldsymbol{H}}_2^{\mathrm{inc}}/\tilde{\boldsymbol{H}}_1^{\mathrm{inc}})$ located at the two slots. The magnetic field varies slowly within the light spot of fundamental mode Gaussian beam, but changes rapidly around the nodal line of HG_{10} mode (see Fig. S2 in the Supplemental Material [32]). Therefore, if HG_{10} mode light is employed to illuminate the POSAs, the relative phase can sharply vary when the POSAs shifts slightly away from the nodal line, thus asymmetric SPPs will be aroused. As an example, we simulate the SPPs excited arisen from POSAs under illumination of HG_{10} mode beam. The SPPs wave is symmetric on both sides of the POSAs when the nodal line is aligned to the center of the POSAs [Fig. 2(c)] and goes to asymmetric when the nodal line is shifted away $\Delta x = 60$ nm [Fig. 2(d)].

In short, we proved directional SPPs were excited by POSAs under the illumination of inhomogeneous optical field. The near-field interaction introduces distinguished initial phase difference between the two adjacent slot antennas leading to constructive interference of SPPs on one side and destructive interference on the other side. We optimized the wavelength by considering the resonance of the slot antenna and introduced HG_{10} mode beam with sharply inhomogeneous field around the nodal line to achieve strongly asymmetric SPPs, depending on the position of the antennas relative to the nodal line of the illuminating HG_{10} mode beam.

A sketch of the experimental setup is depicted in Fig. 3(a). A collimated radially polarized laser ($\lambda = 633$ nm) passes through linear polarizer successively to produce the HG_{10} mode beam and then focused by a microscope objective (20×, NA = 0.75, Olympus) onto the POSA array. The POSAs sample is mounted on a piezostage (P-545.3C8S, Physik Instrumente), allowing for precise movement in the *X*-*Y* plane with nanometric resolution. The propagating SPPs along the air-Ag surface are observed by a leakage radiation microscope composed of an oil-immersion objective lens (100×, NA = 1.45, Olympus) and the microscopic image at the back-focal plane of the objective is captured by a scientific CMOS (sCMOS) camera (Andor, Neo 5.5). Figure 3(b) depicts the optical pattern of incident Gaussian beam, the corresponding pattern of radially polarized beam modulated by an *S*-wave plate and the pattern of HG_{10} mode after the polarizer. The POSA array was fabricated by milling two series of rectangular holes in 50-nm-thick silver film deposited on silica substrate. The SEM image of the POSA array as shown in Fig. 3(c) indicates that length and width of the hole is $l = 100$ and $w = 50$ nm, the center-to-center distance of the slot pair is $d = 120$ nm, and the period of the POSAs is $p = 300$ nm. Typical back-focal plane images of symmetric and asymmetric SPPs are presented in Fig. 3(d). For experimental verification, the POSA array was carefully moved to align its center at the nodal line of HG_{10} beam, the image taken at the back-focal plane of the oil-immersion objective indicated clearly two SPPs arcs symmetrically distributing around a central spot

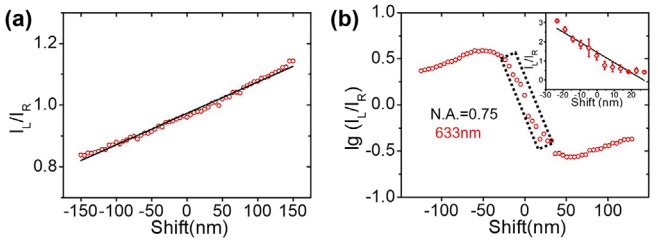

FIG. 4. Nanometric displacement sensing experiment. (a) The red circles represent the experimental measurement of intensity ratio of I_L/I_R depending on the transverse displacement in the displacement range from −150 to 150 nm. The antennas are illuminated by focusing 633 nm Gaussian laser beam with objective lens of 20× and NA = 0.75. (b) Experimentally measured logarithmic ratio of I_L/I_R depending on the transverse displacement of HG_{10} mode spot relative to the center of paired slot antennas. (Inset) The linear fitting of the central part of the measured curve.

corresponding to the forward scattering for the POSAs [top left of Fig. 3(d)]. It is noted that SPPs arcs are spatially separated away from the forward scattering spot, which brings feasibility to retrieve the pure SPPs signal in the back-focal plane. Based on the radius of the SPPs arc, the leakage angle of SPPs can be estimated to be 43.9°, which corresponds to the SPPs along the metal-air interface. For comparison, the antenna was shifted 60 nm to the left to allow the nodal line to align at the right slot, then the left SPPs becomes intense and the right one becomes relatively faint [top right of Fig. 3(d)]. We will demonstrate that the ratio of the left arc intensity to the right one can be used to measure the lateral displacement of the POSAs.

In order to demonstrate the high accuracy of positioning the nanoantenna by monitoring the SPPs leakage, the POSA sample is moved by a piezostage by 5 nm step and the back-focal image is recorded at each step. The intensity of pixels around the SPP arcs are accumulated to acquire the intensity of left-propagating SPPs (I_L) and the right-propagating one (I_R). The ratio $r = I_L/I_R$ is used to characterize the directivity of SPPs excited by POSAs. The transmittance spectrum of the POSA array (Fig. S4 in the Supplemental Material [32]) suggests that a 633 nm laser is a better choice to excite SPPs because slot antenna can be resonantly induced by the incident laser. Figure 4(a) depicts the directivity of SPPs depending on the transverse displacement under the illumination of a 633 nm Gaussian laser beam. In the displacement range from −150 to 150 nm, the directivity is linearly dependent on the displacement and the slope of the function is fitted to be $k_1 = 1.02 \times 10^{-3} \pm 1.2 \times 10^{-5}$ nm^{-1}, which defines the sensitivity of the measurement to the transverse displacement of the antenna. The measurement error of the directivity is estimated to be $\sigma_r = 0.0246$, thus the resolution of the displacement is $\Delta x_{\text{Gaussian}} = 24.1 \pm 0.3$ nm (for details of the derivation, see Sec. 2C in the Supplemental Material [32]). Replacing the Gaussian beam with focused HG_{10} mode beam, the function of SPPs directivity depending on the displacement is presented in Fig. 4(b). Because of the π phase lag for optical field across the nodal line, the slop is negative in the displacement range of [−60, 60] nm. The slope is calculated to be $k_2 = -0.053 \pm 0.005$ nm^{-1} by linear fitting [inset of Fig. 4(b)]. The resolution of the displacement is calculated to be $\Delta x_{\text{HG}} = 3.3 \pm 0.3$ nm. It is clearly demonstrated that resolution of the displacement is dramatically improved when the Gaussian beam is replaced by HG_{10} mode beam. According to the aforementioned interaction model [Eq. (2)], the sensitivity and resolution of the measurement is influenced by the laser wavelength and numerical aperture of the focusing lens, which is also experimentally demonstrated (see Fig. S5 in the Supplemental Material [32]).

We should point out that the resolution estimated above is limited by the vibration of the experimental setup. The error bar as shown in the inset of Fig. 4(b) actually represents the stability of our current experimental setup. To demonstrate the extreme sensing ability of our approach, we try to retrieve the displacement from back-focal plane images of two subsequently recorded positions, which are moved by the instability of the experimental setup. As shown in Fig. S6 in the Supplemental Material [32], the displacements stemming from the vibration of the experimental setup fluctuate from several angstroms to nanometers. The averaged displacement is $|\overline{\Delta x}| = (1/N)\sum \Delta x = 3.02 \pm 0.30$ nm, which is consistent with estimation from the standard error shown in the inset of Fig. 4(b). The smallest displacement among them is $\Delta x = 0.31 \pm 0.030$ nm, which is comparable to resolution of scattering antenna approach [13].

Conclusion.—In summary, we experimentally demonstrated that asymmetric SPPs arise from the interaction between HG_{10} mode optical field and paired slot antennas. The coupling interaction between the two adjacent slot antennas is tuned by the sharp electromagnetic field around the nodal line of the HG_{10} mode. Unlike the previous strategy based on coherent superposition of free space radiations of magnetic and electric dipoles [13,15] or two electric antennas [18], our technique detects the leakage of asymmetric SPPs, other than free scattering, to discriminate the nanometric displacement. The asymmetric optical signal in k space can be retrieved with very high signal-to-noise ratio because the SPPs arc is isolated from the forward scattering background in the k space. Considering the stability of the experimental setup, resolution of our system is demonstrated to be 3.3 ± 0.3 nm, however, the extreme resolution of our approach could be down to angstrom level in the nondeterministic measurement. By integrating two perpendicular POSA arrays onto the wafer or substrate, the samples can be aligned in two dimensions with nanometric resolution, which is potentially applicable in superresolution microscopy, semiconductor lithography, and calibration of nanodevices.

This work was supported by National Natural Science Foundation of China (NSFC) (11674303, 11574293) and Anhui Provincial Science and Technology Major Projects (18030901005). The work was partially carried out at the USTC Center for Micro and Nanoscale Research and Fabrication.

*yhlu@ustc.edu.cn
†wangpei@ustc.edu.cn

[1] H. N. Hansen, K. Carneiro, H. Haitjema, and L. De Chiffre, CIRP Ann. **55**, 721 (2006).
[2] N. Bobroff, Meas. Sci. Technol. **4**, 907 (1993).
[3] J. Gelles, B. J. Schnapp, and M. P. Sheetz, Nature (London) **331**, 450 (1988).
[4] W. E. Moerner and L. Kador, Phys. Rev. Lett. **62**, 2535 (1989).
[5] J. O. Arroyo and P. Kukura, Nat. Photonics **10**, 11 (2016).
[6] F. Balzarotti, Y. Eilers, K. C. Gwosch, A. H. Gynnå, V. Westphal, F. D. Stefani, J. Elf, and S. W. Hell, Science **355**, 606 (2017).
[7] L. Nugent-Glandorf and T. T. Perkins, Opt. Lett. **29**, 2611 (2004).
[8] X. Hao, C. Kuang, Z. Gu, Y. Wang, S. Li, Y. Ku, Y. Li, J. Ge, and X. Liu, Light Sci. Appl. **2**, e108 (2013).
[9] A. J. den Boef, Surf. Topogr. Metrol. Prop. **4**, 023001 (2016).
[10] J. Park, C. Shin, M. Kim, J. Kim, J. Park, J. Kim, C. Jun, Y. Yim, and J. Lee, J. Micro/Nanolithogr. MEMS, MOEMS **13**, 041409 (2014).
[11] N. Yoshimizu, A. Lal, and C. R. Pollock, Opt. Express **18**, 20827 (2010).
[12] G. H. Yuan and N. I. Zheludev, Science **364**, 771 (2019).
[13] A. Bag, M. Neugebauer, P. Woźniak, G. Leuchs, and P. Banzer, Phys. Rev. Lett. **121**, 193902 (2018).
[14] M. Neugebauer, P. Woźniak, A. Bag, G. Leuchs, and P. Banzer, Nat. Commun. **7**, 11286 (2016).
[15] S. Roy, K. Ushakova, Q. van den Berg, S. F. Pereira, and H. P. Urbach, Phys. Rev. Lett. **114**, 103903 (2015).
[16] Y. Wang, Y. Lu, and P. Wang, Opt. Express **26**, 1000 (2018).
[17] L. Wei, A. V. Zayats, and F. J. Rodríguez-Fortuño, Phys. Rev. Lett. **121**, 193901 (2018).
[18] Z. Xi, L. Wei, A. J. L. Adam, H. P. Urbach, and L. Du, Phys. Rev. Lett. **117**, 113903 (2016).
[19] C.-F. Kuo and S.-C. Chu, Opt. Express **25**, 10456 (2017).
[20] M. Neugebauer, S. Nechayev, M. Vorndran, G. Leuchs, and P. Banzer, Nano Lett. **19**, 422 (2018).
[21] Z. Xi, Y. Lu, P. Yao, W. Yu, P. Wang, and H. Ming, Opt. Express **21**, 30327 (2013).
[22] J. Chen, Z. Li, S. Yue, and Q. Gong, Appl. Phys. Lett. **97**, 041113 (2010).
[23] L. Novotny and N. Van Hulst, Nat. Photonics **5**, 83 (2011).
[24] J. Kim *et al.*, Nano Lett. **14**, 3072 (2014).
[25] J. Yang, X. Xiao, C. Hu, W. Zhang, S. Zhou, and J. Zhang, Nano Lett. **14**, 704 (2014).
[26] J. Yang, S. Zhou, C. Hu, W. Zhang, X. Xiao, and J. Zhang, Laser Photonics Rev. **8**, 590 (2014).
[27] J. Lin, J. B. Mueller, Q. Wang, G. Yuan, N. Antoniou, X.-C. Yuan, and F. Capasso, Science **340**, 331 (2013).
[28] Z. Xi, Y. Lu, W. Yu, P. Wang, and H. Ming, J. Opt. **16**, 105002 (2014).
[29] F. J. Rodríguez-Fortuño, G. Marino, P. Ginzburg, D. O'Connor, A. Martínez, G. A. Wurtz, and A. V. Zayats, Science **340**, 328 (2013).
[30] Z. Yang, Y. Fu, J. Yang, C. Hu, and J. Zhang, Nanoscale **10**, 4523 (2018).
[31] D. Lee and D.-S. Kim, Sci. Rep. **6**, 18935 (2016).
[32] See Supplemental Material at http://link.aps.org/supplemental/10.1103/PhysRevLett.124.243901 for detailed derivation of the theoretical model, sample fabrication, optical experiment, data process and FDTD simulations, for the scattering far-field distribution of the slot antenna, and the experiment with fundamental Gaussian mode, which includes Refs. [31,33].
[33] J. D. Jackson, *Classical Electrodynamics* (Wiley, New York, 1999).